CHANNEL ESTIMATION AND LOW-COMPLEXITY BEAMFORMING DESIGN FOR PASSIVE INTELLIGENT SURFACE ASSISTED MISO WIRELESS ENERGY TRANSFER

Deepak Mishra and Håkan Johansson

Div. Commun. Syst., Dept. of Electrical Engineering, Linköping University, 58183 Linköping, Sweden

ABSTRACT

Usage of passive intelligent surface (PIS) is emerging as a low-cost green alternative to massive antenna systems for realizing high energy beamforming (EB) gains. To maximize its realistic utility, we present a novel channel estimation (CE) protocol for PIS-assisted energy transfer (PET) from a multiantenna power beacon (PB) to a single-antenna energy harvesting (EH) user. Noting the practical limitations of PIS and EH user, all computations are carried out at PB having required active components and radio resources. Using these estimates, near-optimal analytical active and passive EB designs are respectively derived for PB and PIS, that enable efficient PET over a longer duration of coherence block. Nontrivial design insights on relative significance of array size at PIS and PB are also provided. Numerical results validating theoretical claims against the existing benchmarks demonstrate that with sufficient passive elements at PIS, we can achieve desired EB gain with reduced active array size at PB.

***Index Terms*—** Wireless energy harvesting, passive beamforming, antenna array, channel estimation, least-squares, phase shifters.

1. INTRODUCTION

Passive intelligent surface (PIS) with reconfigurable reflect-arrays [1, 2] can orient sharp beams toward intended users to achieve similar energy beamforming (EB) gains as by the massive multiple-input-single-output (MISO) systems comprising active arrays. As each element in an active array [3] has its own radio frequency (RF) chain involving several active components like low-noise amplifier, frequency up-converter, and digital-to-analog converter, relative implementation cost of even a massive PIS (where each passive element is just a low-cost printed dipole) is very low [4]. Though PIS has been extensively used in radar systems and space communications, more recently they have gained interest for supporting high data rate and energy sustainability demands of ubiquitously deployed users in 5G networks [4, 5]. This is because PIS can be easily integrated into walls, ceilings, and other reasonable-sized flat-objects near existing transmitter(s) to induce desired phase shifts using PIS-controller for collaboratively altering reflected signal directions. However, as the PIS only comprises passive elements, new channel estimation (CE) and EB protocols are required for maximizing its practical utility as a low-cost green alternative to active arrays in multiantenna systems.

1.1. State-of-the-Art

Considering lightweight and conformal geometry features, the role of PIS attached to walls or ceilings inside a building for improving indoor coverage was first investigated in [2]. These reflect-arrays in PIS can employ varactor diodes or micro-electrical-mechanical systems, whose resonant frequency can be electronically controlled [6] to create desired reflection(s) in intended directions. Lately, a PIS-assisted two-user MISO communication system testbed was also developed in [7] to verify gains due to passive beamforming. Other indoor implementations of PIS include conventional liquid crystal meta-surfaces fabricated via lithography and nanoprinting methods for multiantenna relaying [8], or employing software defined metamaterials [9] as reflect-arrays for supporting nanonetworks applications [10]. On other side, considering active intelligent surface based massive MISO transmission (instead of reflection, as in PIS), authors in [5] derived uplink (UL) data rates at an optimal receiver and quantified the enhancement for indoor communications. In contrast, for outdoor scenarios with PIS having infinite phase resolution passive elements, optimal transmit power allocation and PIS phase shifters (PS) design was investigated in [1] to maximize the downlink (DL) sum-rate. More recently [4], PIS-assisted MISO energy transfer to a single user was studied and a semidefinite relaxation (SDR) based optimal active and passive EB design was proposed. Thus, we notice that research on smart signal processing techniques to maximize the utility of PIS-assisted MISO communications is still in its infancy.

1.2. Motivation and Key Contributions

In the existing literature [1–10], the radio resource-limitations of PIS were ignored and perfect channel state information (CSI) availability was assumed during investigation. Also, their requirements are very different from those of the multiantenna amplify-and-forward relays [1, 4], where active transceiver units are involved. *In fact to our best knowledge, the optimal CE protocol for maximizing the practical efficacy of PIS-assisted energy transfer (PET) over MISO Rician channels has not been investigated yet.* Hence, we present a novel low-complexity optimal CE protocol for maximizing DL received power. Further, since both mean harvested power and achievable rate are non-decreasing in received power [11], *our PIS-limitations-aware EB designs can be applied to both energy transfer and information decoding systems*. This optimal CE protocol with green PIS designs can provide perpetual connectivity for internet-of-things.

The key contribution of this work is three-fold. (1) Novel CE protocol for PET from a multiantenna power beacon (PB) to a single-antenna energy harvesting (EH) user is proposed that neither requires any prior on CSI nor any active participation from PIS. (2) Near-optimal closed-form expressions for transmit (active) and reflect (passive) EB designs are respectively derived for PB and PIS to enable efficient PET over a longer duration of coherence block. These analytical solutions not only enable low-complexity implementation, but also yield nontrivial insights on designing the size of active transmit-array at PB and passive reflect-array at PIS. (3) Numerical investigation is carried out to validate the CE quality, quantify performance gains of PET over benchmarks, and estimate PIS size for achieving a desired EB gain for fixed and optimal CE time.

2. SYSTEM DESCRIPTION

2.1. MISO Wireless Channel Model

We consider a point-to-point MISO wireless system consisting of an N-antenna PB [12], or source $\mathcal{S}$, serving a single-antenna EH user

This research work is funded by the ELLIIT.

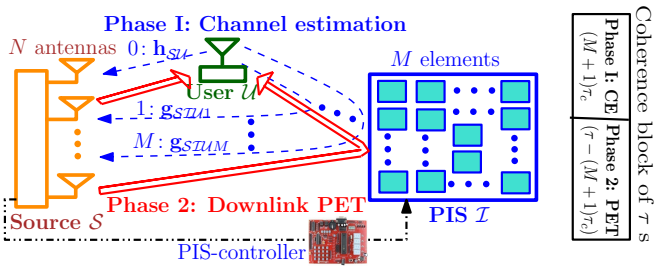

Fig. 1. DL PET from N-antenna $\mathcal{S}$ to $\mathcal{U}$ with help of M-element $\mathcal{I}$ using LS method for estimating $M+1$ channels ($\mathbf{h}_{\mathcal{SU}}, \mathbf{G}_{\mathcal{SIU}}$) in UL.

$\mathcal{U}$. To assist $\mathcal{S}$-to-$\mathcal{U}$ transmission, a PIS $\mathcal{I}$ comprising of M passive elements, or reflect-arrays, is installed on the opposite wall near $\mathcal{S}$, as shown in Fig. 1. These M passive elements [1, 7] at $\mathcal{I}$ act as low resolution PS which can be dynamically reconfigured via a PIS-controller to program the scattering of incident signals from $\mathcal{S}$. Here it may be noted that the negligible strength of the signals reflected two or more times by PIS is ignored [4]. We assume flat quasi-static Rician block fading model [13, Ch 2.2], where the channel impulse response for each link remains invariant during a coherence interval of τ seconds (s) and varies independently across different coherence blocks. So, $\mathcal{S}$-to-$\mathcal{U}$ and $\mathcal{I}$-to-$\mathcal{U}$ channels are represented as below:

$$\mathbf{h}_{ik} = \sqrt{\frac{\beta_{ik} K_{ik}}{K_{ik}+1}} \mathbf{h}_{\mathrm{D}_{ik}} + \sqrt{\frac{\beta_{ik}}{K_{ik}+1}} \mathbf{h}_{\mathrm{S}_{ik}}, \tag{1}$$

$\forall i \in \{\mathcal{S}, \mathcal{I}\}, k \in \mathcal{U}$. Here $\mathbf{h}_{\mathrm{D}_{\mathcal{SU}}} \in \mathbb{C}^{N\times 1}$ and $\mathbf{h}_{\mathrm{D}_{\mathcal{IU}}} \in \mathbb{C}^{M\times 1}$ are deterministic vectors containing specular components [14], β_{ik} models distance-dependent path loss and shadowing based large-scale fading, and K_{ik} is the Rician factor. Whereas, the scattered components $\mathbf{h}_{\mathrm{S}_{\mathcal{SU}}}$ and $\mathbf{h}_{\mathrm{S}_{\mathcal{IU}}}$ are complex Gaussian random vectors with independent and identically distributed (IID) zero-mean unit-variance entries. So, $\mathbf{h}_{ik} \sim \mathbb{CN}\big(\boldsymbol{\mu}_{\mathbf{h}_{ik}}, \mathbf{C}_{\mathbf{h}_{ik}}\big)$, where $\boldsymbol{\mu}_{\mathbf{h}_{\mathcal{SU}}} \in \mathbb{C}^{N\times 1}, \boldsymbol{\mu}_{\mathbf{h}_{\mathcal{IU}}} \in \mathbb{C}^{M\times 1}, \mathbf{C}_{\mathbf{h}_{\mathcal{SU}}} = \frac{\beta_{\mathcal{SU}}}{K_{\mathcal{SU}}+1}\mathbf{I}_N, \mathbf{C}_{\mathbf{h}_{\mathcal{IU}}} = \frac{\beta_{\mathcal{IU}}}{K_{\mathcal{IU}}+1}\mathbf{I}_M$. Likewise the baseband equivalent of Rician fading for $\mathcal{S}$-to-$\mathcal{I}$ link is represented by $\mathbf{H}_{\mathcal{SI}} \in \mathbb{C}^{N\times M}$, whose circularly symmetric complex Gaussian IID random entries have the same variance $\frac{\beta_{\mathcal{SI}}}{K_{\mathcal{SI}}+1}$ and different means as combinedly denoted by the matrix $\boldsymbol{\mu}_{\mathbf{H}_{\mathcal{SI}}} \in \mathbb{C}^{N\times M}$ which models the deterministic component [15] of $\mathcal{S}$-to-$\mathcal{I}$ link, with its large-scale fading parameter as $\beta_{\mathcal{SI}}$ and Rician factor as $K_{\mathcal{SI}}$.

2.2. Adopted PIS Design and Control

Each reflecting element of PIS $\mathcal{I}$ acts as a keyhole combining all the incident signals, and re-scattering this combined signal to behave as a point source [1, 4]. So, with $\alpha_i \in (0, 1)$ and $\theta_i \in (0, 2\pi)$ respectively denoting amplitude reflection coefficient and PS value for the ith passive element of PIS, the diagonal PS matrix whose principal elements represent the passive (reflect) EB design is defined below:

$$\boldsymbol{\Theta} \triangleq \mathrm{diag}\left\{\alpha_1 \mathrm{e}^{j\theta_1}\ \alpha_2 \mathrm{e}^{j\theta_2} \ldots \alpha_M \mathrm{e}^{j\theta_M}\right\} \in \mathbb{C}^{M\times M}. \tag{2}$$

The PIS-controller of $\mathcal{I}$ can dynamically adjust the values of these M α_is and θ_is to orient the underlying reflections from the respective passive elements in the desired directions. Practically, this PIS-controller can be an ultra-low-power micro-controller, designated with only the PS-adjustment role. It is connected to and programmed by $\mathcal{S}$, which has all the required computational and energy resources.

3. PROPOSED CHANNEL ESTIMATION PROTOCOL

In this section we present a novel CE protocol for efficient PET from $\mathcal{S}$ to $\mathcal{U}$. It involves the estimation of channel vectors $\mathbf{h}_{\mathcal{SU}}, \mathbf{h}_{\mathcal{IU}}$, and matrix $\mathbf{H}_{\mathcal{SI}}$ using least-squares (LS) approach as outlined in Section 3.2. But before that, Section 3.1 motivates the need for these estimates in joint active and passive EB designing for efficient PET.

3.1. Channel-Reciprocity Based Downlink MISO PET

As PIS is a passive reflecting unit, assuming channel-reciprocity and adopting the widely investigated time-division duplex (TDD) mode of communication in MISO systems [14, 15], the DL channel coefficients for all the links are obtained by estimating them from the UL pilot transmission from EH $\mathcal{U}$. As depicted in Fig. 1, we consider that each coherence interval of τ s is divided into two subphases, namely, UL CE phase and DL PET phase. Denoting the unit-norm linear precoder or active EB vector at $\mathcal{S}$ by $\mathbf{f}_{\mathrm{A}} \in \mathbb{C}^{N\times 1}$, with its transmit energy signal being $x_e \in \mathbb{C}$, having power $|x_e|^2 = p_e$, the received signal $\mathrm{y}_{\mathcal{U}} \in \mathbb{C}$ at $\mathcal{U}$ during the PET subphase is given by:

$$\begin{aligned} \mathrm{y}_{\mathcal{U}} &= \left(\mathbf{h}_{\mathcal{SU}}^{\mathrm{T}} + \mathbf{h}_{\mathcal{IU}}^{\mathrm{T}}\, \boldsymbol{\Theta}\, \mathbf{H}_{\mathcal{SI}}^{\mathrm{T}}\right) \mathbf{f}_{\mathrm{A}}\, x_e + \mathrm{w}_{\mathcal{U}} \\ &= \left(\mathbf{h}_{\mathcal{SU}}^{\mathrm{T}} + \mathbf{f}_{\mathrm{P}}^{\mathrm{T}}\, \mathbf{G}_{\mathcal{SIU}}^{\mathrm{T}}\right) \mathbf{f}_{\mathrm{A}}\, x_e + \mathrm{w}_{\mathcal{U}}, \end{aligned} \tag{3}$$

where M diagonal entries of $\boldsymbol{\Theta}$ in (2) denote the passive EB or PS vector $\mathbf{f}_{\mathrm{P}} \in \mathbb{C}^{M\times 1}$ at $\mathcal{I}$, $\mathbf{G}_{\mathcal{SIU}} \triangleq \mathbf{H}_{\mathcal{SI}}\, \mathrm{diag}\left\{\mathbf{h}_{\mathcal{IU}}^{\mathrm{T}}\right\} \in \mathbb{C}^{N\times M}$ represents the cascaded channel matrix, and $\mathrm{w}_{\mathcal{U}}$ is the received additive white Gaussian noise (AWGN) with zero-mean and variance $\sigma^2_{\mathrm{w}_{\mathcal{U}}}$. Ignoring EH from noise power, the received signal power at $\mathcal{U}$ is:

$$\mathcal{P}_{\mathcal{U}} = |\mathrm{y}_{\mathcal{U}}|^2 \approx p_e \left|\left(\mathbf{h}_{\mathcal{SU}}^{\mathrm{T}} + \mathbf{f}_{\mathrm{P}}^{\mathrm{T}}\, \mathbf{G}_{\mathcal{SIU}}^{\mathrm{T}}\right) \mathbf{f}_{\mathrm{A}}\right|^2. \tag{4}$$

Since, the precoding vectors, $\mathbf{f}_{\mathrm{A}}$ and $\mathbf{f}_{\mathrm{P}}$ require information on $\mathbf{h}_{\mathcal{SU}}$ and $\mathbf{G}_{\mathcal{SIU}}$, next we outline LS method to obtain them via UL CE.

3.2. Novel Binary Reflection Controlled LS Channel Estimation

With PIS $\mathcal{I}$ not having any radio resources of its own and being programmed by $\mathcal{S}$ using PIS-controller, we propose a binary-reflection (*full* or *no*) controlled LS CE protocol which runs over total duration of $(M+1)\,\tau_c$ to obtain LS estimator (LSE) for $M+1$ channel vectors, having N elements each, as denoted by $\mathbf{h}_{\mathcal{SU}}$ and M columns $\mathbf{g}_{\mathcal{SIU}i}, \forall i \in \mathcal{M} = \{1, 2, \ldots, M\}$, of $\mathbf{G}_{\mathcal{SIU}}$. *This binary model is adopted because it takes care of the fact that PIS does not have any active components, and thus, PB has to itself estimate all the* $M+1$ *channel vectors* ($\mathbf{h}_{\mathcal{SU}}, \mathbf{g}_{\mathcal{SIU}i}, \forall i \in \mathcal{M}$), *one-by-one.* As depicted in Fig. 1, throughout the CE phase duration of $(M+1)\,\tau_c \leq \tau$ (in seconds) [15, 16], $\mathcal{U}$ transmits a pilot signal x_p, having power $p_c = |x_p|^2$, to $\mathcal{S}$. So, during the ith subphase of duration τ_c s, only ith passive element of $\mathcal{I}$ is in *full-reflection or ON* mode with its amplitude coefficient set as $\alpha_i = 1$ to aid $\mathcal{S}$ in estimating $\mathbf{g}_{\mathcal{SIU}i}$, while all other elements, being in *no-reflection or OFF* mode, set their coefficients to $\alpha_k = 0, \forall k \neq i$. However, due to practical restrictions we may not be able to realize perfect *ON/OFF* reflection modes. Hence, with non-negative constants ϵ_1 and ϵ_0 respectively modeling these realistic implementation errors in *ON* and *OFF* modes, entries of combined $\mathcal{I}$'s PS matrix $\boldsymbol{\Phi} \in \mathbb{R}_{\geq 0}^{M\times(M+1)}$ during CE phase are:

$$[\boldsymbol{\Phi}]_{i,m} \triangleq \begin{cases} 1-\epsilon_1, & (i=m) \wedge (m \neq 1) \\ 0+\epsilon_0, & (i \neq m) \vee (m = 1) \end{cases}, \forall i \in \mathcal{M}, m \in \mathcal{M}_+, \tag{5}$$

where $\mathcal{M}_+ \triangleq \mathcal{M} \cup \{M+1\}$. So, each column's M entries in $\boldsymbol{\Phi}$ represent the practical amplitude coefficient values, with all PS set as $\theta_i = 0, \forall i \in \mathcal{M}$. Therefore, using (3), the combined received signal matrix $\mathbf{Y}_{\mathcal{S}} \in \mathbb{C}^{N\times(M+1)}$ at $\mathcal{S}$ during CE phase can be written as:

$$\mathbf{Y}_{\mathcal{S}} = \left(\left(\left(\mathbf{h}_{\mathcal{SU}} \otimes \mathbf{1}_{1\times(M+1)}\right) + \mathbf{G}_{\mathcal{SIU}}\, \boldsymbol{\Phi}\right) \otimes x_p\right) + \mathbf{W}_{\mathcal{S}}. \tag{6}$$

where $\otimes$ is Kronecker product operator and $\mathbf{W}_{\mathcal{S}}$ is AWGN matrix with variance $\sigma^2_{\mathrm{w}_{\mathcal{S}}}$ for all entries. Denoting 1st column vector of $\mathbf{Y}_{\mathcal{S}}$ by $\mathbf{y}_1$, we rewrite $\mathbf{Y}_{\mathcal{S}}=\big[\mathbf{y}_1 \;\; \overline{\mathbf{Y}}_{\mathcal{S}}\big]$ with $\overline{\mathbf{Y}}_{\mathcal{S}}$ as its last M column vectors. Similarly, we can redefine $\mathbf{W}_{\mathcal{S}} = \big[\mathbf{w}_1 \;\; \overline{\mathbf{W}}_{\mathcal{S}}\big]$, $\mathbf{\Phi} = [\epsilon_0 \mathbf{1}_{M\times 1} \;\; \overline{\mathbf{\Phi}}]$, and $\mathbf{X}_p \triangleq \overline{\mathbf{\Phi}} \otimes x_p \in \mathbb{C}^{M\times M}$. Using these in (6) we obtain:

$$\mathbf{y}_1 = (\mathbf{h}_{\mathcal{SU}} + \epsilon_0\, \mathbf{G}_{\mathcal{SIU}}\, \mathbf{1}_{M\times 1})\, x_p + \mathbf{w}_1, \tag{7a}$$

$$\overline{\mathbf{Y}}_{\mathcal{S}} = x_p\, (\mathbf{h}_{\mathcal{SU}} \otimes \mathbf{1}_{1\times M}) + \mathbf{G}_{\mathcal{SIU}}\, \mathbf{X}_p + \overline{\mathbf{W}}_{\mathcal{S}}. \tag{7b}$$

Therefore, the LS estimate of $\mathcal{S}$-to-$\mathcal{U}$ channel $\mathbf{h}_{\mathcal{SU}}$ as obtained using the pseudoinverse $x_p^\dagger \triangleq \frac{x_p^*}{p_c \tau_c}$ of pilot signal x_p is defined below [17]:

$$\widehat{\mathbf{h}}_{\mathcal{SU}} = \mathbf{y}_1\, x_p^\dagger = \mathbf{h}_{\mathcal{SU}} + \widetilde{\mathbf{h}}_{\mathcal{SU}}, \tag{8}$$

where $\widetilde{\mathbf{h}}_{\mathcal{SU}} \triangleq \widehat{\mathbf{h}}_{\mathcal{SU}} - \mathbf{h}_{\mathcal{SU}} = \epsilon_0\, \mathbf{G}_{\mathcal{SIU}}\, \mathbf{1}_{M\times 1} + \frac{\mathbf{w}_1\, x_p^*}{p_c\, \tau_c}$ represents the CE error. Using this LS estimate $\widehat{\mathbf{h}}_{\mathcal{SU}}$ of $\mathbf{h}_{\mathcal{SU}}$, the LS estimate for the cascaded channel matrix $\mathbf{G}_{\mathcal{SIU}}$, as obtained using the pseudoinverse $\mathbf{X}_p^\dagger \triangleq \mathbf{X}_p^{\mathrm{H}} \left(\mathbf{X}_p\, \mathbf{X}_p^{\mathrm{H}}\right)^{-1}$ of $\mathbf{X}_p$ [17], is represented below:

$$\widehat{\mathbf{G}}_{\mathcal{SIU}} = \left(\overline{\mathbf{Y}}_{\mathcal{S}} - x_p \left(\widehat{\mathbf{h}}_{\mathcal{SU}} \otimes \mathbf{1}_{1\times M}\right)\right) \mathbf{X}_p^\dagger = \mathbf{G}_{\mathcal{SIU}} + \widetilde{\mathbf{G}}_{\mathcal{SIU}}, \tag{9}$$

where $\widetilde{\mathbf{G}}_{\mathcal{SIU}} \triangleq \left(\overline{\mathbf{W}}_{\mathcal{S}} - x_p \left(\widetilde{\mathbf{h}}_{\mathcal{SU}} \otimes \mathbf{1}_{1\times M}\right)\right) \mathbf{X}_p^\dagger$ representing error in estimating $\mathbf{G}_{\mathcal{SIU}} = \mathbf{H}_{\mathcal{SI}}\, \mathrm{diag}\big\{\mathbf{h}_{\mathcal{IU}}^{\mathrm{T}}\big\}$ shows that CE in PET is more prone to errors than in conventional MISO communications without PIS. This critical aspect will be numerically verified in Section 5.1.

4. JOINTLY OPTIMAL ACTIVE AND PASSIVE EB DESIGN

Here we first recall the existing EB designs assuming perfect CSI at $\mathcal{S}$, and start with mathematically formulating the problem of interest:

$$\mathcal{O}_{\mathrm{J1}}\colon \max_{\mathbf{f}_{\mathrm{A}}, \mathbf{f}_{\mathrm{P}}} \;\; \mathcal{P}_{\mathcal{U}}, \;\; \text{s. t. } (\mathrm{C1})\colon \|\mathbf{f}_{\mathrm{A}}\|^2 \le 1, \;\; (\mathrm{C2})\colon \big|[\mathbf{f}_{\mathrm{P}}]_i\big| = 1, \forall i \in \mathcal{M}.$$

Since for any passive EB design $\mathbf{f}_{\mathrm{P}}$, maximum ratio transmission (MRT) yields the optimal active EB at $\mathcal{S}$, we set optimal $\mathbf{f}_{\mathrm{A}}$ as below:

$$\mathbf{f}_{\mathrm{A}_{\mathrm{opt}}^{\mathrm{id}}} = \frac{\mathbf{h}_{\mathcal{SU}}^* + \mathbf{G}_{\mathcal{SIU}}^*\, \mathbf{f}_{\mathrm{P}}^*}{\|\mathbf{h}_{\mathcal{SU}}^* + \mathbf{G}_{\mathcal{SIU}}^*\, \mathbf{f}_{\mathrm{P}}^*\|}, \tag{10}$$

and using which $\mathcal{O}_{\mathrm{J1}}$ gets reduced to the below equivalent problem:

$$\mathcal{O}_{\mathrm{J2}}\colon \max_{\mathbf{f}_{\mathrm{P}}} \;\; \mathcal{P}_{\mathcal{U}_{\mathrm{A}}^{\mathrm{opt}}} \triangleq p_e \left\|\mathbf{h}_{\mathcal{SU}}^{\mathrm{T}} + \mathbf{f}_{\mathrm{P}}^{\mathrm{T}}\, \mathbf{G}_{\mathcal{SIU}}^{\mathrm{T}}\right\|^2, \;\; \text{s. t. } (\mathrm{C2}).$$

To resolve non-convexity of $\mathcal{O}_{\mathrm{J2}}$, authors in [4] proposed a SDR based solution, as obtained numerically using CVX [18], followed by randomization method to construct a rank-one solution. Though it has been shown to perform very well, the complexity of solving this problem [4, Problem (P5)] with $M+1$ variables and constraints is in the order of $O\big((M+1)^6\big)$ [19, sec. 6.6.3]. To avoid this very high complexity, which is very critical in PIS-assisted communications with $M \gg 1$, we next present a closed-form solution for passive EB design, whose quality is later verified against this SDR one in Fig. 2.

4.1. Proposed Closed-form Joint EB Design

The received RF power at $\mathcal{U}$ in $\mathcal{O}_{\mathrm{J2}}$ for optimal active EB under ideal scenario of perfect CSI availability can be rewritten as below:

$$\mathcal{P}_{\mathcal{U}_{\mathrm{A}}^{\mathrm{opt}}} = p_e \left(\left\|\mathbf{h}_{\mathcal{SU}}^{\mathrm{T}}\right\|^2 + \left\|\mathbf{f}_{\mathrm{P}}^{\mathrm{T}}\, \mathbf{G}_{\mathcal{SIU}}^{\mathrm{T}}\right\|^2 + 2\left\langle \mathbf{h}_{\mathcal{SU}}^{\mathrm{T}}, \mathbf{f}_{\mathrm{P}}^{\mathrm{T}}\, \mathbf{G}_{\mathcal{SIU}}^{\mathrm{T}} \right\rangle\right), \tag{11}$$

where $\langle \mathbf{a}, \mathbf{b} \rangle$ is the standard inner product between vectors. Thus, to ensure that the reflected signals from $\mathcal{I}$ get coherently added up $\mathcal{U}$ with ones received directly from $\mathcal{S}$, we design the passive EB vector $\mathbf{f}_{\mathrm{P}}$ by setting the amplitude coefficients to the maximum value 1, i.e., $\alpha_i = 1, \forall i \in \mathcal{M}$, and then phases are set as to ensure that reflected signal ($\mathcal{S}$-to-$\mathcal{I}$-to-$\mathcal{U}$) received at $\mathcal{U}$ aligns with direct one ($\mathcal{S}$-to-$\mathcal{U}$). Hence using (11), analytical expression for proposed passive EB is:

$$\mathbf{f}_{\mathrm{P}_{\mathrm{opt}}^{\mathrm{id}}} = \exp\left\{-j \,\underline{/\mathbf{G}_{\mathcal{SIU}}^{\mathrm{T}}\, \mathbf{h}_{\mathcal{SU}}^*}\right\}, \qquad \text{with} \quad j = \sqrt{-1}. \tag{12}$$

Thus, our proposed solution just requires single computational step in (12)*, and thereby, yields a significant reduction in complexity.* Below we present a key analytical insight out of our novel EB solution.

Remark 1 *The proposed EB design ensures the constructive interference of the reflected and directly received signals, respectively from $\mathcal{I}$ and $\mathcal{S}$, at $\mathcal{U}$, i.e., collectively received power, $\mathcal{P}_{\mathcal{U}_{\mathrm{A}}^{\mathrm{opt}}}$, is more than the sum of individual powers, $p_e\Big(\big\|\mathbf{h}_{\mathcal{SU}}^{\mathrm{T}}\big\|^2 + \big\|\mathbf{f}_{\mathrm{P}}^{\mathrm{T}}\, \mathbf{G}_{\mathcal{SIU}}^{\mathrm{T}}\big\|^2\Big)$.*

Now with the proposed EB for perfect CSI availability given by (10) and (12), the practical joint active and passive EB designs under CE errors as obtained in closed-form using LSE for $\mathbf{h}_{\mathcal{SU}}$ and $\mathbf{G}_{\mathcal{SIU}}$ are:

$$\mathbf{f}_{\mathrm{A}_{\mathrm{opt}}^{\mathrm{pra}}} \triangleq \frac{\widehat{\mathbf{h}}_{\mathcal{SU}}^* + \widehat{\mathbf{G}}_{\mathcal{SIU}}^*\, \mathbf{f}_{\mathrm{P}_{\mathrm{opt}}^{\mathrm{pra}}}^*}{\left\|\widehat{\mathbf{h}}_{\mathcal{SU}}^* + \widehat{\mathbf{G}}_{\mathcal{SIU}}^*\, \mathbf{f}_{\mathrm{P}_{\mathrm{opt}}^{\mathrm{pra}}}^*\right\|}, \;\; \mathbf{f}_{\mathrm{P}_{\mathrm{opt}}^{\mathrm{pra}}} \triangleq \exp\left\{-j \,\underline{/\widehat{\mathbf{G}}_{\mathcal{SIU}}^{\mathrm{T}}\, \widehat{\mathbf{h}}_{\mathcal{SU}}^*}\right\}. \tag{13}$$

Next we use these expressions to develop nontrivial design insights.

4.2. Insights on Relative Active and Passive EB Gains

Recalling from Section 3, the practically realizable effective harvested power at $\mathcal{U}$, considering the energy spent in CE, is given by:

$$\mathcal{E}_{\mathrm{H}} \triangleq \tau_e\, \eta\, p_e \left|\left(\mathbf{h}_{\mathcal{SU}}^{\mathrm{T}} + \mathbf{f}_{\mathrm{P}_{\mathrm{opt}}^{\mathrm{pra}}}^{\mathrm{T}}\, \mathbf{G}_{\mathcal{SIU}}^{\mathrm{T}}\right) \mathbf{f}_{\mathrm{A}_{\mathrm{opt}}^{\mathrm{pra}}}\right|^2 - (M+1)\, \tau_c\, p_c, \tag{14}$$

where $\tau_e \triangleq \tau - (M+1)\, \tau_c$ is the time for PET and η is rectification efficiency [20, 21] of EH unit at $\mathcal{U}$. As shown later in Fig. 5, for maximizing PET efficiency, *τ_c has to be selected optimally while resolving the underlying CE-quality versus delivered-energy-quantity tradeoff*. Further, as η is non-decreasing in received power [20], and the passive EB $\mathbf{f}_{\mathrm{P}_{\mathrm{opt}}^{\mathrm{pra}}}$ ensures constructive interference of reflected and direct signals (Remark 1), $\mathcal{E}_{\mathrm{H}}$ in (14) can be lower-bounded as:

$$\mathcal{E}_{\mathrm{H}} \ge \tau_e\, \eta\, (p_{\mathrm{A}} + p_{\mathrm{P}}) - (M+1)\, \tau_c\, p_c, \tag{15}$$

where $p_{\mathrm{A}} \triangleq \frac{p_e \mathbf{h}_{\mathcal{SU}}^{\mathrm{T}} \widehat{\mathbf{h}}_{\mathcal{SU}}^*}{\left\|\widehat{\mathbf{h}}_{\mathcal{SU}}^*\right\|}$ and $p_{\mathrm{P}} \triangleq \frac{p_e \mathbf{f}_{\mathrm{P}_{\mathrm{opt}}^{\mathrm{pra}}}^{\mathrm{T}} \mathbf{G}_{\mathcal{SIU}}^{\mathrm{T}} \widehat{\mathbf{G}}_{\mathcal{SIU}}^* \mathbf{f}_{\mathrm{P}_{\mathrm{opt}}^{\mathrm{pra}}}^*}{\left\|\widehat{\mathbf{G}}_{\mathcal{SIU}}^* \mathbf{f}_{\mathrm{P}_{\mathrm{opt}}^{\mathrm{pra}}}^*\right\|}$ respectively are the contribution of active and passive EB gains. Below we discuss how to use (15) for designing the PIS and PB array sizes.

Remark 2 *For independent channels [14, 15], with larger active array size N at PB, $\mathcal{E}_{\mathrm{H}}$ gets enhanced due to higher summation terms in received power p_{A}. Whereas, as each passive element at PIS contributes to a term in all N summation terms of p_{P}, we can design PIS with sufficiently large M to achieve desired EB gain with reduced N.*

This critical design aspect of saving significant cost by reducing active array size at PB by increasing M at PIS is studied in Section 5.2.

5. NUMERICAL RESULTS AND CONCLUSIONS

Here, we evaluate the achievable EB gains during PET under CE errors. Unless otherwise stated, we have used $N = 10, M = 20$, $\tau = 1$ms and $\tau_c = \frac{0.01\tau}{M+1}$, $\epsilon_1 = 0$, $\epsilon_0 = 10^{-3}$, $p_e = 30$dBm, $p_c = -10$dBm, $\sigma^2_{\mathrm{w}_{\mathcal{S}}} = \sigma^2_{\mathrm{w}_{\mathcal{U}}} = \sigma^2 \triangleq 10^{-20}$ Joule (J) [14], $\eta = 0.7$, $K_{\mathcal{SU}} = K_{\mathcal{IU}} = 0$ [4], $K_{\mathcal{SI}} = 10$, $\delta = \frac{3\times 10^8}{2f}$, and $\beta_{ik} = \frac{G_i G_k \varpi}{d_{ik}^\varrho}, \forall i, k \in \{\mathcal{S}, \mathcal{U}, \mathcal{I}\}$, where $\varpi = \left(\frac{\delta}{2\pi}\right)^2$ being average channel attenuation at

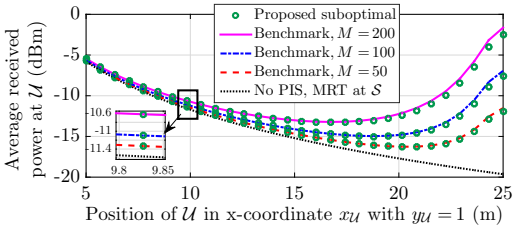

Fig. 2. Validating near-optimality of proposed analytical EB designs.

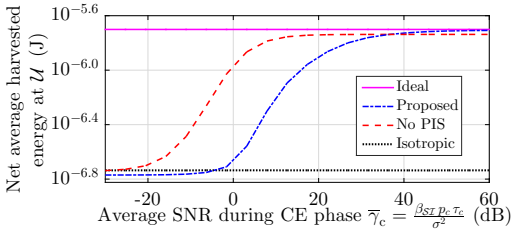

Fig. 3. Validating the quality of proposed LSE for different SNRs.

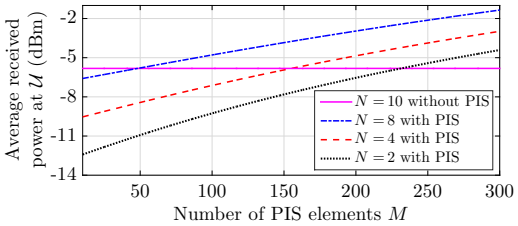

Fig. 4. Insights on PIS size needed to reduce active array size at PB.

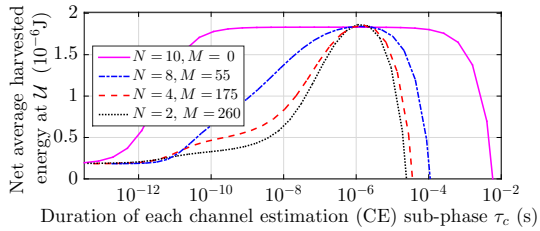

Fig. 5. Impact of CE time τ_c on PET performance for varying N, M.

unit reference distance with δ being the inter-element separation at PIS and PB [14], $f = 915$ MHz [22] being transmit frequency, d_{ik} is i to k distance, $G_{\mathcal{S}} = G_{\mathcal{U}} = 0$dBi, $G_{\mathcal{I}} = 5$dBi [4], and $\varrho = 2$ is the path loss exponent [20]. The specular components of Rician fading channels for all links are modeled using [15, eq. (2)] and we have set $L = 1$ and $g_i = 1, \forall i$, in that. Further, we have considered rectangular topology [4] for positioning $\mathcal{S}, \mathcal{I}$, and $\mathcal{U}$ inside a room (cf. Fig. 1) with d_x and d_y being the lengths of its two sides in meters (m). As $\mathcal{S}$ and $\mathcal{I}$, being d_x distance apart, lie on the one side with their respective coordinates being $(x_{\mathcal{S}}, y_{\mathcal{S}})$ and $(x_{\mathcal{I}}, y_{\mathcal{I}})$, $\mathcal{U}$ lies on the other parallel side d_y distance apart with coordinates $(x_{\mathcal{U}}, y_{\mathcal{U}})$. Hence, $x_{\mathcal{S}} = 0, x_{\mathcal{I}} = d_x, y_{\mathcal{S}} = y_{\mathcal{I}} = 0, y_{\mathcal{U}} = d_y, d_{\mathcal{SI}} = d_x, d_{\mathcal{SU}} = \sqrt{x_{\mathcal{U}}^2 + d_y^2}$, and $d_{\mathcal{IU}} = \sqrt{(d_x - x_{\mathcal{U}})^2 + d_y^2}$. We use $x_{\mathcal{U}} = 5$m, $d_x = 10$m, and $d_y = 1$m. Lastly, all results here have been generated after taking average over 10^4 independent channel realizations.

5.1. Verification of Analytical Claims

We start with validating the near-optimality of our proposed analytical EB design $(\mathbf{f}_{\mathrm{A}^{\mathrm{id}}_{\mathrm{opt}}}, \mathbf{f}_{\mathrm{P}^{\mathrm{id}}_{\mathrm{opt}}})$ against the SDR-based benchmark design [4] for different PIS sizes M. From Fig. 2, we observe that the performance gap between the benchmark and our closed-form design is less than $1\%, 2\%$, and 3.5%, for M as $50, 100$, and 200, respectively. *This corroborates the practical near-optimality of our proposed computationally-efficient analytical EB designs in making a fast decision, and hence, allowing longer time for DL PET phase.* Further, as compared to the *'No PIS'* case, the proposed EB designs for PET with M as $50, 100$, and 200, providing an average improvement of around 2dB, 4.1dB, and 7.5dB, respectively, demonstrates the significance of using PIS. Lastly, we also observe that the signal coverage of $\mathcal{U}$ by $\mathcal{S}$ is improved by using PIS $\mathcal{I}$ because it alleviates the signal attenuation problem over larger $d_{\mathcal{SU}}$ (as plotted via higher $x_{\mathcal{U}}$) by allowing $\mathcal{U}$ to receive strong reflected signals from other end.

Next via Fig. 3, we validate the quality of proposed LSEs, $\widehat{\mathbf{h}}_{\mathcal{SU}}$ and $\widehat{\mathbf{G}}_{\mathcal{SIU}}$, against increasing average signal-to-noise-ratio (SNR) $\overline{\gamma}_c = \frac{\beta_{\mathcal{SI}} p_c \tau_c}{\sigma^2}$ values during CE phase. With average effective harvested power $\mathcal{E}_{\mathrm{H}}$ at EH $\mathcal{U}$ (cf. (14)) as the performance validation metric for estimating the goodness of LSEs, we have also plotted the perfect CSI (no CE error) and isotropic [15] transmission cases to respectively present upper and lower bounds on average value of $\mathcal{E}_{\mathrm{H}}$. As observed from Fig. 3, the quality of $\mathcal{E}_{\mathrm{H}}$ performance for proposed LSEs improves with increasing SNR because the underlying CE error reduces, and for SNRs greater than 45dB, the corresponding practical performance approaches as that with perfect CSI availability. Here, we also notice that *CE accuracy is more critical in PET as compared to 'No PIS' scenario because higher CE time (pr SNR) is needed in the former case to learn additional (reflected) channel matrix* $\mathbf{G}_{\mathcal{SIU}}$. So, we conclude that optimal CE protocol plays key role in realizing the practical merits of PIS-assisted communications.

5.2. Key Optimal Design Insights

In this part we bring out the designing criteria for selecting the size M for PIS which allows much cheaper implementation with passive elements alone, and array size N for PB that can provide higher EB gains at the cost of active energy consumption. Specifically, via Fig. 4, we try to find out the PIS size that can meet the EB gain requirements with lower array size N at PB. It is noted that on ignoring CE errors, PET with $M = 52$ and $N = 8$ can achieve the same performance as that for $N = 10$ without PIS. Likewise, for achieving the latter performance for PET with $N = 2$ and $N = 4$, the number of passive elements required at PIS are $M = 239$ and $M = 163$, respectively. Further, *for reducing* 6 *active antenna from* $N = 10$ *and* $N = 8$ *designs, we respectively need to include an additional* 163 *and* 187 *passive elements at PIS.* This additional PIS size actually depends on the $\mathcal{U}$'s location. So, in contrast to $x_{\mathcal{U}} = 5$m, when $\mathcal{U}$ moves closer to PIS, with $x_{\mathcal{U}} = \{6, 7, 8, 9\}$m, we need fewer $M = \{222, 175, 127, 96\}$ passive elements for reducing N from 10 to 2.

Lastly, we conclude this paper by shedding some key insights on optimal CE time τ_c maximizing $\mathcal{E}_{\mathrm{H}}$, defined in (14), under practical CE errors. From Fig. 5, where the variation of average harvested energy $\mathcal{E}_{\mathrm{H}}$ with τ_c is plotted for different N values, it can be observed that it is unimodal in τ_c. Also, $\mathcal{E}_{\mathrm{H}} = 0$ for $\tau_c = \frac{\tau}{M+1}$, and the value at $\tau_c = 0$s represents the isotropic transmission performance. It is interesting to note that the optimal CE time $\tau_{c_{opt}} \approx 10^{-6}$s $= \frac{\tau}{1000}$ remains same irrespective of the sizes (N, M) of PB and PIS. Further, the values of M in Fig. 5 have been selected to achieve the same average $\mathcal{E}_{\mathrm{H}}$ performance for underlying different N values. In comparison to the results in Fig. 4, here we notice that, under CE errors, larger sized PIS is needed to meet the same EB requirements as with $N = 10$. Specifically, in practice around 8% more passive elements are required when using LSEs to design the joint active and passive EB vectors in (13) instead of using perfect CSI for EB in (10), (12).

Thus, we summarize that *setting CE time as* $\tau_c \approx \frac{\tau}{1000}$ *for obtaining LSEs can yield significant EB gains* (Fig. 5). Also, a larger sized low-cost PIS can be chosen to have smaller active array size N at PB to implement EB in an efficient way noting limitations of PIS.

6. REFERENCES

[1] C. Huang, A. Zappone, M. Debbah, and C. Yuen, "Achievable rate maximization by passive intelligent mirrors," in *Proc. IEEE ICASSP*, Calgary, Canada, Apr. 2018, pp. 3714–3718.

[2] L. Subrt and P. Pechac, "Intelligent walls as autonomous parts of smart indoor environments," *IET Commun.*, vol. 6, no. 8, pp. 1004–1010, May 2012.

[3] A. Yazdan, J. Park, S. Park, T. A. Khan, and R. W. Heath, "Energy-efficient massive MIMO: Wireless-powered communication, multiuser MIMO with hybrid precoding, and cloud radio access network with variable-resolution ADCs," *IEEE Microw. Mag.*, vol. 18, no. 5, pp. 18–30, July 2017.

[4] Q. Wu and R. Zhang, "Intelligent reflecting surface enhanced wireless network: Joint active and passive beamforming design," in *Proc. IEEE GLOBECOM*, Abu Dhabi, UAE, Dec. 2018, pp. 1–6.

[5] S. Hu, F. Rusek, and O. Edfors, "Beyond massive MIMO: The potential of data transmission with large intelligent surfaces," *IEEE Trans. Signal Process.*, vol. 66, no. 10, pp. 2746–2758, May 2018.

[6] S. V. Hum and J. Perruisseau-Carrier, "Reconfigurable reflectarrays and array lenses for dynamic antenna beam control: A review," *IEEE Trans. Ant. Prop.*, vol. 62, no. 1, pp. 183–198, Jan. 2014.

[7] X. Tan, Z. Sun, J. M. Jornet, and D. Pados, "Increasing indoor spectrum sharing capacity using smart reflect-array," in *Proc. IEEE ICC*, Kuala Lumpur, Malaysia, May 2016, pp. 1–6.

[8] S. Foo, "Liquid-crystal reconfigurable metasurface reflectors," in *Proc. IEEE Int. Symp. on Ant. Prop. (ISAP)*, San Diego, USA, July 2017, pp. 2069–2070.

[9] T. J. Cui, M. Q. Qi, J. Zhao X. Wan, and Q. Cheng, "Coding metamaterials, digital metamaterials and programmable metamaterials," *Light: Science & Applications*, vol. 3, no. 10, pp. e218, 2014.

[10] X. Tan, Z. Sun, D. Koutsonikolas, and J. M. Jornet, "Enabling indoor mobile millimeter-wave networks based on smart reflect-arrays," in *Proc. IEEE INFOCOM*, Honolulu, USA, Apr. 2018, pp. 270–278.

[11] D. Mishra and G. C. Alexandropoulos, "Transmit precoding and receive power splitting for harvested power maximization in MIMO SWIPT systems," *IEEE Trans. Green Commun. Netw.*, vol. 2, no. 3, pp. 774–786, Sept. 2018.

[12] K. Huang and V. K. N. Lau, "Enabling wireless power transfer in cellular networks: Architecture, modeling and deployment," *IEEE Trans. Wireless Commun.*, vol. 13, no. 2, pp. 902–912, Feb. 2014.

[13] M. K. Simon and M.-S. Alouini, *Digital communication over fading channels*, vol. 95, New Jersey: John Wiley & Sons, 2nd edition, 2005.

[14] S. Kashyap, E. Björnson, and E. G. Larsson, "On the feasibility of wireless energy transfer using massive antenna arrays," *IEEE Trans. Wireless Commun.*, vol. 15, no. 5, pp. 3466–3480, May 2016.

[15] Y. Zeng and R. Zhang, "Optimized training design for wireless energy transfer," *IEEE Trans. Commun.*, vol. 63, no. 2, pp. 536–550, Feb. 2015.

[16] D. Mishra and H. Johansson, "Efficacy of multiuser massive MISO wireless energy transfer under IQ imbalance and channel estimation errors over rician fading," in *Proc. IEEE ICASSP*, Calgary, Canada, Apr. 2018, pp. 3844–3848.

[17] S. M. Kay, *Fundamentals of Statistical Signal processing: Estimation Theory*, vol. 1, Upper Saddle River, NJ: Prentice Hall, 1993.

[18] Michael Grant and Stephen Boyd, "CVX: Matlab software for disciplined convex programming," version 2.1. http://cvxr.com/cvx, Mar. 2014.

[19] A. Ben-Tal and A. Nemirovski, *Lectures on modern convex optimization: analysis, algorithms, and engineering applications*, vol. 2, Siam, 2001.

[20] D. Mishra and S. De, "Utility maximization models for two-hop energy relaying in practical RF harvesting networks," in *Proc. IEEE ICC*, Paris, France, May 2017, pp. 41–46.

[21] P. N. Alevizos and A. Bletsas, "Sensitive and nonlinear far field RF energy harvesting in wireless communications," *IEEE Trans. Wireless Commun.*, vol. 17, no. 6, pp. 3670–3685, June 2018.

[22] "Powercast datasheet – P1110B Powerharvester receiver," `http://www.powercastco.com./documentation/`, accessed Oct. 23, 2017.